WATER RESOURCES RESEARCH, VOL. 45, W03417, doi:10.1029/2008WR007099, 2009

Determination of surface flow paths from gridded elevation data

Stefano Orlandini[1] and Giovanni Moretti[1]

Received 18 April 2008; revised 5 October 2008; accepted 9 December 2008; published 24 March 2009.

[1] Surface flow paths are obtained from gridded elevation data by connecting grid cell centers along predetermined flow directions. These flow directions are commonly determined using single and multiple flow direction algorithms. It remains, however, unclear whether multiple flow direction algorithms, which introduce artificial dispersion, can be used to describe surface flow paths and gravity-driven processes across a terrain without causing unrealistic flow dispersion. To explore this issue, a unified algorithm for the determination of flow directions has been developed, and new methods for the validation of the resulting surface flow paths are introduced. The unified algorithm makes it possible, by setting appropriate parameters, to perform local or path-based analyses and to experiment with different combinations of single and multiple flow directions in a morphologically significant manner. The new validation methods use drainage systems delineated from contour elevation data as a reference and take into consideration the overlap between these systems and those obtained from gridded elevation data. The unified algorithm is presented, and the results are evaluated for selected case studies in order to provide guidance on the use of surface flow path algorithms based on gridded elevation data.

Citation: Orlandini, S., and G. Moretti (2009), Determination of surface flow paths from gridded elevation data, *Water Resour. Res.*, *45*, W03417, doi:10.1029/2008WR007099.

1. Introduction

[2] Surface flow paths describe the way in which water and sediments move on the land surface under the effect of gravity. In principle, these paths can easily be determined from contour elevation data as those lines that intersect contour lines at right angles [*Maxwell*, 1870]. However, this problem presents practical difficulties that can only be overcome by means of complex numerical techniques [e.g., *Dawes and Short*, 1994; *Moretti and Orlandini*, 2008]. Moreover, a classical flow net derived by using flow lines is not suited to natural landscapes because flow strips continually merge or split, and the flow net has to be modified by amalgamating excessively small elements and subdividing excessively large elements [*Moore and Grayson*, 1991]. The practical difficulties inherent in the analysis of contour elevation data have led hydrologists to develop and use more efficient and straightforward digital elevation models, such as gridded (regular network) or triangulated irregular network digital elevation models [e.g., *Orlandini and Rosso*, 1998; *Ivanov et al.*, 2004]. While the delineation of drainage basins and the construction of flow nets from contour elevation data have been dealt with by *Moretti and Orlandini* [2008], the present study focuses on the determination of surface flow paths from gridded elevation data.

[3] Surface flow paths are obtained from gridded elevation data by connecting grid cell centers along predetermined flow directions [e.g., *Gallant and Wilson*, 2000]. The earliest and simplest method for specifying these flow directions is to assign a pointer from each cell to one of its eight neighbors, either adjacent or diagonal, in the direction of the steepest downward slope. This method was introduced by *O'Callaghan and Mark* [1984] and *Marks et al.* [1984] and is commonly designated as D8 (eight flow directions). The D8 approach, however, has two major limitations: (1) the flow direction from each cell is restricted to only eight possibilities separated by $\pi/4$ rad (when square cells are used), and (2) a drainage area, which originates over a two-dimensional cell, is treated as a point source (nondimensional) and projected downslope by a line (one-dimensional) [*Moore and Grayson*, 1991]. To mitigate these limitations, alternative methods have been proposed [e.g., *Fairfield and Leymarie*, 1991; *Freeman*, 1991; *Quinn et al.*, 1991; *Lea*, 1992; *Costa-Cabral and Burges*, 1994; *Tarboton*, 1997; *Orlandini et al.*, 2003; *Seibert and McGlynn*, 2007]. A critical review of methods developed in the early 1990s is given by *Tarboton* [1997]. More recent methods are also considered in this study by focusing attention on the use of single and multiple flow directions. Single flow direction methods allow flow from a cell to only one downslope nearest-neighbor cell, while multiple flow direction methods allow flow to be distributed to more than one downslope nearest-neighbor cells [e.g., *Gallant and Wilson*, 2000, pp. 61 and 64].

[4] Multiple flow direction methods have been introduced and developed to improve the computation of drainage areas and the description of surface flow paths over morphologically divergent terrains [*Freeman*, 1991; *Quinn et al.*, 1991]. However, these methods produce artificial dispersion of flow from a cell to neighboring cells at a lower elevation, which may be inconsistent with the physical definition of drainage area [*Maxwell*, 1870; *Leopold et al.*, 1964, p. 131].

[1] Dipartimento di Ingegneria Meccanica e Civile, Università degli Studi di Modena e Reggio Emilia, Modena, Italy.

0043-1397/09/2008WR007099$09.00

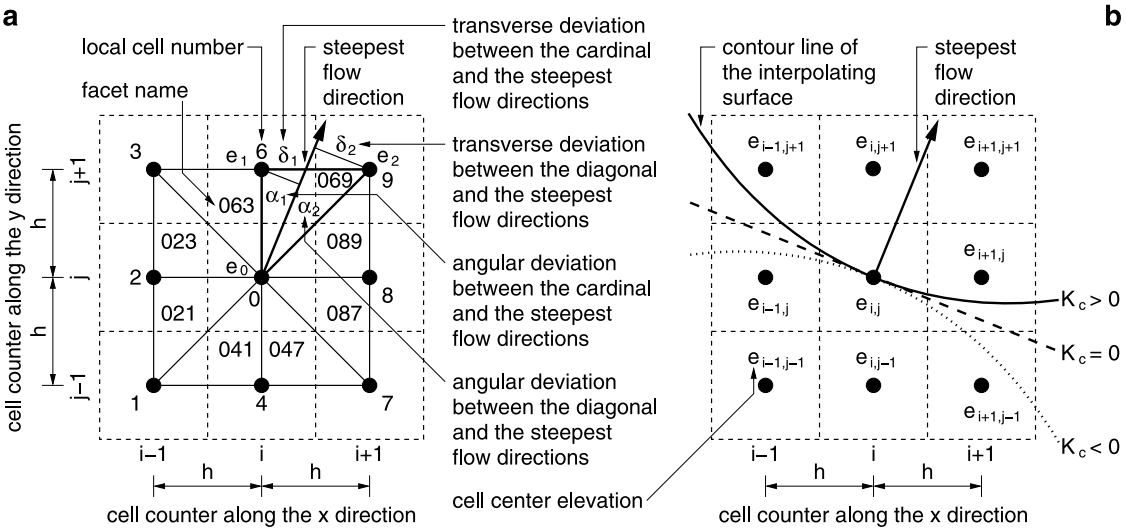

Figure 1. Sketch of the elementary computational systems used to determine (a) flow directions and (b) plan (or contour) curvatures.

Tarboton [1997] presented a multiple flow direction method that attempted to minimize artificial dispersion, arguing that physical dispersion of water, sediments, and solutes, if necessary, should be modeled separately. Nonetheless, this method still produces some artificial dispersion, to a degree that is variable depending on flow direction. *Orlandini et al.* [2003] agreed with *Tarboton*'s [1997] approach, noting that single flow direction methods are nondispersive and may provide a better description of nondispersive processes, especially to the extent that grid bias can be reduced using flow path approaches.

[5] It is emphasized here that artificial dispersion in terrain analysis is clearly inconsistent with the purely morphological definition of drainage area based on *Maxwell*'s [1870] theory, and may also be inconsistent with any broader definition of drainage area based on contribution of water, sediments, and solutes, since physical dispersion inherent in transport processes across a terrain may not obey the same laws as artificial dispersion. The role of physical dispersion of water, sediments, and solutes across a terrain is not questioned here, but rather the principle is followed that a sound study of these processes should be based on a purely morphological description of the terrain and a separate description of the transport processes occurring across the terrain. In this perspective, moderately dispersive methods based on *Tarboton*'s [1997] approach are considered, and inconsistencies with the morphological definition of drainage area due to artificial dispersion are investigated. If present, inconsistencies affecting moderately dispersive methods are expected to affect also more markedly dispersive methods [e.g., *Quinn et al.*, 1991; *Seibert and McGlynn*, 2007]. However, it is stressed here that deliberately dispersive methods do not conform with the principle mentioned above, and thus are not within the focus of this study.

[6] Inferences on the accuracy of surface flow paths have been widely made by considering the resulting drainage areas, but this strategy may not be entirely sound since a correct value of the drainage area at a given location does not necessarily reflect a correct determination of surface flow paths across the upslope terrain. New validation methods are developed in this study by using drainage systems delineated from contour elevation data as a reference, and by considering the overlap between these systems and those obtained from gridded elevation data. Numerical experiments are carried out by using (1) highly accurate (contour and gridded) elevation data generated from a lidar survey of an area in the Italian Alps, (2) the methods for the analysis of contour elevation data developed by *Moretti and Orlandini* [2008], and (3) a unified algorithm for the determination of surface flow paths from gridded elevation data that makes it possible, by setting appropriate parameters, local or path-based analyses and a hybrid morphology-driven use of single and multiple flow directions across the processed terrain. The unified algorithm is described in section 2; the validation methods are presented in section 3; the case studies are reported in sections 4; and the discussion of the results is provided in section 5.

2. Determination of Surface Flow Paths

[7] A unified algorithm for the determination of surface flow paths and drainage areas from gridded elevation data is developed by combining (1) the method for the computation of steepest flow directions introduced by *Tarboton* [1997], (2) the local and path-based analyses described by *Orlandini et al.* [2003], and (3) a hybrid use of single and multiple flow directions based on the determination of the local plan (or contour) curvature given by *Zevenbergen and Thorne* [1987]. A general formulation is described in sections 2.1–2.5. Relevant cases derived by setting appropriate parameters from this general formulation are highlighted in section 2.6.

2.1. Steepest Flow Directions

[8] Following the method introduced by *Tarboton* [1997], the elementary computational system sketched in Figure 1a is used to compute the steepest (downward) flow direction for all cells of a grid-based digital elevation model. Square cells having size equal to h are considered and a block-centered scheme with each elevation value taken to represent the elevation of the center of the corresponding cell is

Table 1. Determinations of the Variables Used in the Flow Direction Algorithm[a]

	Facet							
Variable	021	023	063	069	089	087	047	041
e_0	$e_{i,j}$	$e_{i,j}$	$e_{i,j}$	$e_{i,j}$	$e_{i,j}$	$e_{i,j}$	$e_{i,j}$	$e_{i,j}$
e_1	$e_{i-1,j}$	$e_{i-1,j}$	$e_{i,j+1}$	$e_{i,j+1}$	$e_{i+1,j}$	$e_{i+1,j}$	$e_{i,j-1}$	$e_{i,j-1}$
e_2	$e_{i-1,j-1}$	$e_{i-1,j+1}$	$e_{i-1,j+1}$	$e_{i+1,j+1}$	$e_{i+1,j+1}$	$e_{i+1,j-1}$	$e_{i+1,j-1}$	$e_{i-1,j-1}$
p_1	2	2	6	6	8	8	4	4
p_2	1	3	3	9	9	7	7	1
σ	+1	−1	+1	−1	+1	−1	+1	−1

[a]Algorithm is described in section 2; computational system is shown in Figure 1a.

adopted. Eight planar triangular facets are formed between the cell and its eight neighboring cells. The three-dimensional geometry of each facet is characterized by the elevations e_i ($i = 0,1,2$). These elevations are arranged such that e_0 is in the center point, e_1 is in the point to the side, and e_2 is in the diagonal point. For a generic triangular facet, the slope (downward) can be represented by the vector (s_1,s_2), where $s_1 = (e_0-e_1)/h$ and $s_2 = (e_1-e_2)/h$. The direction (angle with the cardinal direction of the facet) and magnitude of the maximum slope in the facet are $r = \arctan(s_2/s_1)$ and $s_{\max} = (s_1^2 + s_2^2)^{1/2}$, respectively. If r is not in the angle range of the facet at the center point [0,π/4 rad], then r needs to be set as the direction along the appropriate edge and $s_{\max}$ assigned as the slope along the edge. If $r < 0$, then r and $s_{\max}$ are set equal to 0 and s_1, respectively. If $r > \pi/4$ rad, then r and $s_{\max}$ are set equal to $\pi/4$ rad and $(e_0-e_2)/(\sqrt{2}\ h)$, respectively. Table 1 gives the node elevations corresponding to the corners of each of the triangular facets used to compute slopes and angles. The steepest flow direction associated with a grid cell is determined in the direction of the steepest downward slope on the eight triangular facets centered on that cell. Equalities are resolved by selecting (among all the equal possibilities) the steepest flow direction along the facet that is processed first, starting conventionally from facet 021 and proceeding in a clockwise manner. Equalities are rare and normally unimportant as long as high-accuracy gridded elevation data representing real terrains are considered.

2.2. Least Angular and Transverse Deviations

[9] The steepest flow direction computed at a given grid cell can vary continuously as an angle between 0 and 2π rad and does not generally follow one of the cardinal (0, $\pi/2$, π, and $3\pi/2$ rad) or diagonal ($\pi/4$, $3\pi/4$, $5\pi/4$, and $7\pi/4$ rad) directions that can be selected. Possible flow directions from a given grid cell are identified by a pointer p indicating the local cell number of the draining cell. The pointers associated to the cardinal and diagonal directions of the facet containing the steepest flow direction are denoted as p_1 and p_2, respectively, and reported in Table 1. A possible criterion for approximating the steepest flow direction with a single flow direction is to ensure the least angular deviation (LAD). As shown in Figure 1a, the angular deviations produced when approximating the steepest flow direction by the cardinal and the diagonal directions are α_1 and α_2, respectively, where $\alpha_1 = r$ and $\alpha_2 = \pi/4$ rad$-r$. The LAD criterion determines that the direction identified by p_1 is selected if $\alpha_1 \leq \alpha_2$, whereas the direction identified by p_2 is selected if $\alpha_1 > \alpha_2$. A different criterion introduced by *Orlandini et al.* [2003] ensures the least transverse deviation (LTD). The term "transverse" replaces the term "transversal" used by *Orlandini et al.* [2003]. Transverse deviation indicates the linear distance between the center of the draining cell and the path along the steepest flow direction originating at the center of the drained cell. As shown in Figure 1a, the transverse deviations produced when approximating the steepest flow direction by the cardinal and the diagonal directions are $\delta_1 = h \sin\alpha_1$ and $\delta_2 = \sqrt{2}\ h \sin\alpha_2$, respectively. The LTD criterion determines that the direction identified by p_1 is selected if $\delta_1 \leq \delta_2$, whereas the direction identified by p_2 is selected if $\delta_1 > \delta_2$. The LTD criterion is theoretically as justifiable as the LAD criterion. The former highlights the deviations at the end of the elemental flow paths, and the latter at the beginning (Figure 1a).

2.3. Local and Path-Based Analyses

[10] Local and path-based deviations between surface flow paths extending along the selected flow directions and the steepest flow directions are described in this section by considering a flow path determined by single flow directions and not connected to other converging flow paths. The extension to the general case where converging flow paths and/or multiple flow directions occur is provided in section 2.4. A sign σ is assigned to each deviation that may occur in the eight triangular facets of the elementary computational system so as to allow a meaningful (arithmetic) accumulation of deviations along a flow path. Possible values of σ are reported in Table 1. At the first cell along a given path ($k = 1$), the local (angular or transverse) deviations associated to pointers p_1 and p_2 are denoted as $\delta_1(1)$ and $\delta_2(1)$, respectively. Using the notation introduced in section 2.2, $\delta_1(1) = \alpha_1$ and $\delta_2(1) = \alpha_2$ when angular deviations are considered, whereas $\delta_1(1) = \delta_1$ and $\delta_2(1) = \delta_2$ when transverse deviations are considered. The corresponding cumulative (angular or transverse) deviations are initialized as $\delta_1^+(1) = \sigma\ \delta_1(1)$ and $\delta_2^+(1) = -\sigma\ \delta_2(1)$. If single flow directions are used, the flow direction from the first cell along the path ($k = 1$) is selected among the two options associated to pointers p_1 and p_2 so as to minimize the absolute value of the cumulative (angular or transverse) deviation, and the cumulative (angular or transverse) deviation conveyed to the downslope cell $\delta^+(1)$ is computed.

$$\text{If } \left|\delta_1^+(1)\right| \leq \left|\delta_2^+(1)\right|, \text{ then } p = p_1,\ \delta^+(1) = \delta_1^+(1). \quad (1)$$

$$\text{If } \left|\delta_1^+(1)\right| > \left|\delta_2^+(1)\right|, \text{ then } p = p_2, \delta^+(1) = \delta_2^+(1). \quad (2)$$

On subsequent cells along a given path ($k = 2,3,\ldots$), the local (angular or transverse) deviations associated to

pointers p_1 and p_2 are denoted as $\delta_1(k)$ and $\delta_2(k)$, respectively. Using the notation introduced in section 2.2, $\delta_1(k) = \alpha_1$ and $\delta_2(k) = \alpha_2$ when angular deviations are considered, whereas $\delta_1(k) = \delta_1$ and $\delta_2(k) = \delta_2$ when transverse deviations are considered. The corresponding cumulative (angular or transverse) deviations are computed as

$$\delta_1^+(k) = \sigma\delta_1(k) + \lambda\delta^+(k-1) \tag{3}$$

and

$$\delta_2^+(k) = -\sigma\delta_2(k) + \lambda\delta^+(k-1), \tag{4}$$

where λ is a weighting factor whose value is between 0 and 1, and $\delta^+(k-1)$ is the cumulative (angular or transverse) deviation conveyed to the kth cell along the path and determined by the selection of flow directions along the upslope path. The flow direction from the kth cell along the path ($k = 2,3,\ldots$) is selected among the two options associated to pointers p_1 and p_2 so as to minimize the absolute value of the (angular or transverse) deviation, and the cumulative (angular or transverse) deviation conveyed to the downslope cell $\delta^+(k)$ is computed.

$$\text{If } \left|\delta_1^+(k)\right| \le \left|\delta_2^+(k)\right|, \text{ then } p = p_1,\ \delta^+(k) = \delta_1^+(k). \tag{5}$$

$$\text{If } \left|\delta_1^+(k)\right| > \left|\delta_2^+(k)\right|, \text{ then } p = p_2,\ \delta^+(k) = \delta_2^+(k). \tag{6}$$

The term $\delta^+(k-1)$ in equations (3) and (4) is given by (1) and (2), for $k = 2$ ($k-1 = 1$), and by (5) and (6), for $k > 2$ ($k-1 > 1$). For $\lambda = 0$, the selection of the flow directions is based only on the local (angular or transverse) deviations $\delta_1(k)$ and $\delta_2(k)$ ($k = 1,2,\ldots$). For $0 < \lambda < 1$ upslope (angular or transverse) deviations are partially considered. For $\lambda = 1$, full consideration of the upslope (angular or transverse) deviations is retained.

2.4. Single and Multiple Flow Directions

[11] If multiple (double in the cases examined in this study) flow directions are used, both flow directions from a cell, associated to pointers p_1 and p_2, are selected and drainage area is dispersed along these flow directions in proportion to the weights

$$w_1 = \frac{\left|\delta_2^+\right|}{\left|\delta_1^+\right| + \left|\delta_2^+\right|} \tag{7}$$

and

$$w_2 = \frac{\left|\delta_1^+\right|}{\left|\delta_1^+\right| + \left|\delta_2^+\right|}, \tag{8}$$

respectively, where δ_1^+ and δ_2^+ are the cumulative (angular or transverse) deviations associated to pointers p_1 and p_2. It is specified here that the grid cell counter k used in section 2.3 cannot be maintained when (converging flow paths and/or) multiple flow directions occur. In order to determine surface flow paths and compute drainage areas, grid cells located in flat or depressed areas are raised so as to ensure for them a flow direction with a small positive (downward) slope and are then processed in the order of descending elevation. The cumulative (angular or transverse) deviation conveyed from the upslope neighboring cells to a considered cell is computed as

$$\delta^+ = \sum_i w^{(i)} A^{(i)} \delta^{+(i)} \Big/ \sum_i w^{(i)} A^{(i)}, \tag{9}$$

where the summations extend to all the upslope neighboring cells ($i = 1,2,\ldots$), $w^{(i)}$ ($i = 1,2,\ldots$) is the weight associated to the flow conveyed from the cell (i) to the considered cell, $A^{(i)}$ ($i = 1,2,\ldots$) is the area drained by the cell (i) plus the area of the cell (i) itself, and $\delta^{+\ (i)}$ ($i = 1,2,\ldots$) is the cumulative (angular or transverse) deviation conveyed from the cell (i) to the considered cell. The product $w^{(i)} A^{(i)}$ ($i = 1,2,\ldots$) provides the area conveyed from the cell (i) to the considered cell, whereas $\sum_i w^{(i)} A^{(i)}$ provides the area totally drained by the considered cell. One can note that $w^{(i)} = 0$ if the cell (i) does not drain into the considered cell, $0 < w^{(i)} < 1$ if the cell (i) partially drains into the considered cell (this case being possible only if a multiple flow direction is used for cell (i)), and $w^{(i)} = 1$ if the cell (i) entirely drains into the considered cell. Equation (9) provides the general expression of the cumulative (angular or transverse) deviation, denoted as $\delta^+(k-1)$ in equations (3) and (4), that must be used when converging flow paths occur and/or either single or multiple flow directions are used.

2.5. Combinations of Single and Multiple Flow Directions

[12] As a general heuristic principle, surface flow paths and gravity-driven processes across a terrain can be described by using single flow directions over convergent terrains and multiple flow directions over divergent terrains. The plan (or contour) curvature, defined as the curvature of contour lines, provides a measure of the morphological convergence of the terrain, and can therefore be applied to determine whether to use single or multiple flow directions for each grid cell. As suggested by *Zevenbergen and Thorne* [1987], a partial quadratic equation expressing the elevation e as a function of planar coordinates x and y can be used to interpolate (by Lagrange polynomials) the nine cell elevations $e_{I,J}$ ($I = i-1, i, i+1; J = j-1, j, j+1$) of a 3×3 submatrix such as that sketched in Figure 1b, and plan curvature can be found by differentiating this quadratic equation and solving the resulting equation for the central point of the 3×3 submatrix. The resulting local plan curvature associated to a given grid cell is

$$K_c = \frac{e_{xx}e_y^2 - 2e_{xy}e_xe_y + e_{yy}e_x^2}{\left(e_x^2 + e_y^2\right)^{3/2}}, \tag{10}$$

where $e_x = \partial e/\partial x \approx (e_{i+1,j} - e_{i-1,j})/(2\,h)$, $e_y = \partial e/\partial y \approx (e_{i,j+1} - e_{i,j-1})/(2\,h)$, $e_{xx} = \partial^2 e/\partial x^2 \approx (e_{i+1,j} - 2\,e_{i,j} + e_{i-1,j})/h^2$, $e_{yy} = \partial^2 e/\partial y^2 \approx (e_{i,j+1} - 2\,e_{i,j} + e_{i,j-1})/h^2$, $e_{xy} = \partial^2 e/(\partial x \partial y) \approx (-e_{i-1,j+1} + e_{i+1,j+1} + e_{i-1,j-1} - e_{i+1,j-1})/(4\,h^2)$, and h is the grid spacing along the x and y directions. Single or multiple flow directions are selected at each grid cell depending on whether the value of K_c given by (10) exceeds or not a fixed threshold value K_{ct}, respectively. By varying

Table 2. Relevant Parameterizations of the Unified Flow Direction Algorithm[a]

Method	LAD/LTD[b], λ	K_{ct}	ND/D/H[c]
	Local Methods		
D8	LAD, $\lambda = 0$	$(-\infty, \min(K_c))$	ND
D∞	LAD, $\lambda = 0$	$[\max(K_c), +\infty)$	D
	Path-Based Methods		
D8-LTD	LTD, $\lambda = 1$	$(-\infty, \min(K_c))$	ND
D∞-LTD	LTD, $\lambda = 1$	$[\max(K_c), +\infty)$	D
D8/∞-LTD	LTD, $\lambda = 1$	$(-\infty, +\infty)$	H

[a]Algorithm is described in section 2.
[b]LAD, least angular deviation; LTD, least transverse deviation.
[c]ND, nondispersive; D, dispersive; H, hybrid.

this threshold value K_{ct}, the algorithm can exhibit a range of dispersive behavior, from uniformly nondispersive (K_{ct} less than the minimum value of K_c computed over the processed cells) to uniformly dispersive (K_{ct} greater than or equal to the maximum value of K_c computed over the processed cells). For instance, by setting K_{ct} equal to zero, the algorithm selects single flow directions over locally convergent terrains and multiple flow directions over locally divergent terrains.

2.6. Relevant Cases

[13] The algorithm described in sections 2.1–2.5 makes it possible, by setting appropriate parameters, to perform local (LAD criterion, $\lambda = 0$) or path-based (LTD criterion, $\lambda = 1$) analyses, and to experiment a range of hybrid nondispersive-dispersive behavior ($-\infty < K_{ct} < +\infty$), from a spatially uniform nondispersive behavior ($K_{ct} < \min(K_c)$) to a spatially uniform dispersive behavior ($K_{ct} \geq \max(K_c)$). As reported in Table 2, (1) the LAD, local, uniformly nondispersive algorithm is the D8 method proposed by *O'Callaghan and Mark* [1984] and *Marks et al.* [1984], (2) the LAD, local, uniformly dispersive algorithm is the D∞ method proposed by *Tarboton* [1997], (3) the LTD, path-based, uniformly nondispersive algorithm is the D8-LTD method proposed by *Orlandini et al.* [2003], and (4) the LTD, path-based, uniformly dispersive algorithm is a variant of the D∞ method denoted here as D∞-LTD. The LAD and LTD criteria, as well as the weighting factor λ, have comprehensively been investigated by *Orlandini et al.* [2003], who ultimately advocated the LTD criterion with $\lambda = 1$. Attention is focused in this study on the selection of the plan curvature threshold K_{ct}, which allows for a morphologically meaningful use of single (nondispersive) and multiple (dispersive) flow directions across a terrain. Path-based methods (LTD criterion, $\lambda = 1$) including the D8-LTD method ($K_{ct} < \min(K_c)$), the D∞-LTD method ($K_{ct} \geq \max(K_c)$), and a hybrid of the two denoted here as D8/∞-LTD ($-\infty < K_{ct} < +\infty$) are considered (Table 2). The D8 method (LAD criterion, $\lambda = 0$, $K_{ct} < \min(K_c)$) and the D∞ method (LAD criterion, $\lambda = 0$, $K_{ct} \geq \max(K_c)$) are also considered so as to provide a comparison between the advanced methods investigated in this study and the simpler methods currently in use (Table 2).

3. Validation Methods

[14] As shown in Figure 2, the algorithm presented in section 2 can be validated by considering draining line segments connecting assigned points (P_L and P_R) and comparing, for each draining line segment, the drainage basins obtained from gridded elevation data (denoted as grid drainage basin or GDB) and the corresponding drainage basin delineated from contour elevation data (denoted as contour drainage basin or CDB). Surface flow paths obtained using a single flow direction algorithm are considered in Figure 2 in order to present a simple initial case. The general case in which either a single or a multiple flow direction algorithm are used is illustrated at the end of this section. The skeleton construction techniques developed by *Moretti and Orlandini* [2008] are used to accurately delineate drainage basins from contour elevation data so that the obtained results can be taken as a reference.

[15] New metrics for the validation of surface flow paths obtained from gridded elevation data are defined by considering the "degree of belonging" of grid cells to the drainage basins delineated from contour elevation data. Three contributions of grid cells to areas accumulated along surface flow paths are distinguished: (1) areas A_1 belonging to the CDB, but not to the GDB, (2) areas A_2 belonging to both the CDB and the GDB (intersection), and (3) areas A_3 belonging to the GDB, but not to the CDB. As shown in Figure 2, a grid cell draining (through the surface flow paths obtained from gridded elevation data) outside the line segment P_LP_R (underlying both the CDB and the GDB) does not belong to the GDB, but may belong partially or entirely to the CDB. The degree of belonging of this cell to the CDB ranges between 0 (for external cells) to 1 (for internal cells) and provides a measure of the cell proportion (as a part of the whole) contributing to area A_1 (pattern with diagonal lines at $+\pi/4$ rad). A grid cell draining (through the surface flow paths determined from gridded elevation data) inside the line segment P_LP_R belongs to the GDB and may belong partially or entirely to the CDB. The degree of belonging of this cell to the CDB ranges from 0 (external cell) to 1 (internal cell) and provides a measure of the cell proportion (as a part of the whole) contributing to area A_2

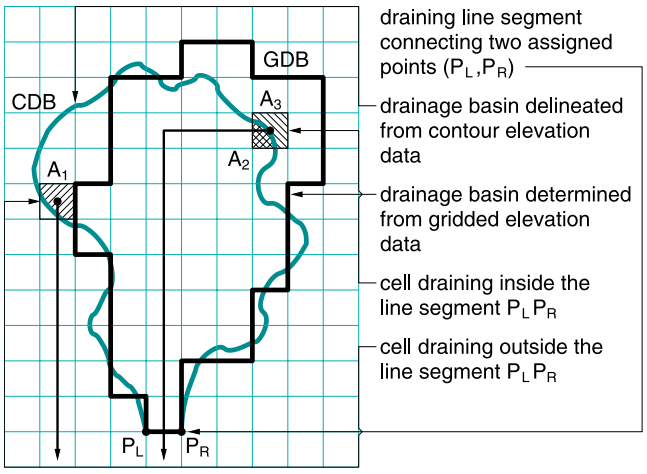

Figure 2. Sketch of a drainage basin delineated from contour elevation data (denoted as contour drainage basin or CDB) and a drainage basin determined from gridded elevation data (denoted as grid drainage basin or GDB) for the same draining line segment P_LP_R connecting two assigned points (P_L, P_R).

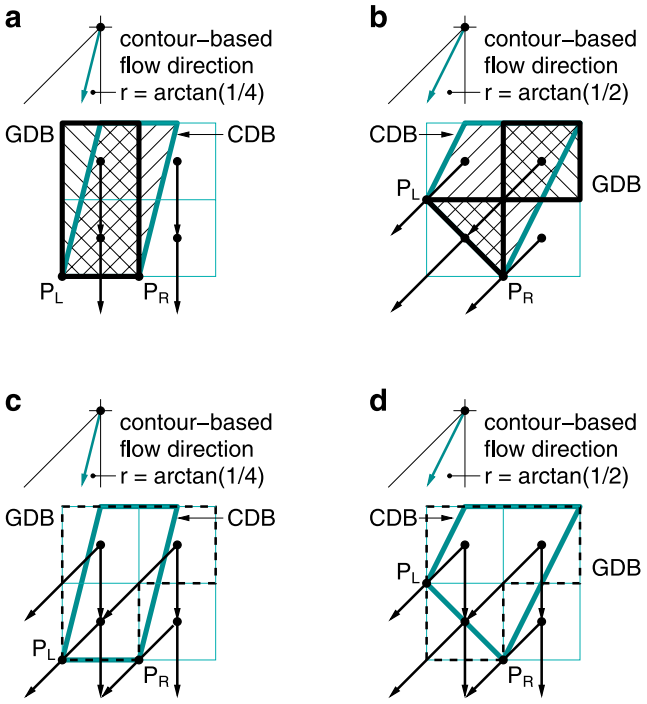

Figure 3. Solution of four simple cases obtained by considering (a and b) single or (c and d) multiple flow direction algorithms along with contour-based flow directions closest to the cardinal (Figures 3a and 3c) or the diagonal (Figures 3b and 3d) directions. Numerical features are reported in Table 3.

(pattern with crossing diagonal lines at $+\pi/4$ and $-\pi/4$ rad). The complementary cell proportion, which does not belong to the CDB, necessarily contributes to area A_3 (pattern with diagonal lines at $-\pi/4$ rad).

[16] The total contributions to areas A_1, A_2, and A_3 can be computed through the following four steps:

[17] 1. A region that is sufficiently large to contain both the CDB and the GDB is considered. A weight equal to the degree of belonging of the cell to the CDB is assigned to each grid cell within the considered region. This weight ranges from 0 (external cells) to 1 (internal cells). Surface flow paths are determined from gridded elevation data, using an algorithm selected among those presented in section 2, and the area drained by the line segment P_LP_R is computed. The result obtained provides area A_2.

[18] 2. Area A_1 is computed as the difference between the area of the CDB ($A_1 + A_2$) obtained from contour elevation data and area A_2 obtained from the previous step.

[19] 3. To each grid cell (within the region containing both the CDB and the GDB) a weight equal to 1 is assigned. Surface flow paths are determined from gridded elevation data (using the algorithm selected in the first step) and the area drained by the line segment P_LP_R is computed. The result obtained provides area ($A_2 + A_3$).

[20] 4. Area A_3 is computed as the difference between area ($A_2 + A_3$) obtained from the previous step and area A_2 obtained from the first step.

[21] Areas A_1, A_2, and A_3 allow for the definition of two types of errors, both relative to the area of the CDB ($A_1 + A_2$), which is taken as a reference. Type 1 relative error $|(A_2 + A_3) - (A_1 + A_2)|/(A_1 + A_2)$ accounts for the absolute difference between the areas of the CDB and the GDB, and is ultimately expressed as

$$E_1 = \frac{|A_1 - A_3|}{A_1 + A_2}. \tag{11}$$

Type 2 relative error accounts for the total nonoverlapping area ($A_1 + A_3$), and is expressed as

$$E_2 = \frac{A_1 + A_3}{A_1 + A_2}. \tag{12}$$

One can note that error E_1 is just an indicator of the absolute difference between the drainage areas of the CDB and the GDB, independently of the locations of elementary contributions to these drainage areas, whereas error E_2 also considers the nonoverlapping between the two drainage basin determinations. From equations (11) and (12) it is apparent that $E_1 > 0$ if and only if the CDB and the GDB display different drainage areas, whereas $E_2 > 0$ if and only if the CDB and the GDB display different configurations (which do not necessarily imply different drainage areas). Since $E_2 \geq E_1$, it follows that $E_2 = 0$ implies $E_1 = 0$ and indicates a perfect overlap between the CBD and the GDB.

[22] The computation of A_1, A_2, A_3, E_1, and E_2 when either a single or a multiple flow direction algorithm are used, is illustrated by describing the four simple cases shown in Figure 3. Each of these cases is defined by considering four cells with centers lying on a planar slope draining along an assigned flow direction r (section 2.1). For any selected draining line segment P_LP_R, the CDB can easily be identified by considering flow lines extending along the assigned direction r and passing through the points P_L and P_R. The four case studies shown in Figure 3 are obtained by considering the D8 single (Figures 3a and 3b) or the D∞ multiple (Figures 3c and 3d) flow direction methods (path-based methods are not relevant for these four-cell systems), along with contour-based flow directions closest to the cardinal ($r \leq \pi/8$ rad, $\alpha_1 \leq \alpha_2$, Figures 3a and 3c) or to the diagonal ($r > \pi/8$ rad, $\alpha_1 > \alpha_2$, Figures 3b and 3d) directions. The numerical features of the four cases shown in Figure 3 are reported in Table 3. A thick solid line is used to delineate the GDB determined from the D8 single flow direction method (Figures 3a and 3b), whereas a thinner dashed line is used to delineate grid cells contributing (entirely or partially) to the GDB determined from the D∞ multiple flow direction method (Figures 3c and 3d).

[23] In the case shown in Figure 3a (where $r = \arctan(1/4)$), one can obtain that $A_1 = 1/2\ h^2$, $A_2 = 3/2\ h^2$, $A_3 = 1/2\ h^2$, $E_1 = 0$, and $E_2 = 1/2$. While E_1 is insensitive to the (angular) deviation between steepest and selected flow directions, E_2 is able to capture and express meaningfully the difference between the CDB and the GDB. In the case shown in Figure 3b (where $r = \arctan(1/2)$), one can obtain that $A_1 = h^2$, $A_2 = 5/4\ h^2$, $A_3 = 1/4\ h^2$, $E_1 = 1/3$, and $E_2 = 5/9$. Surface flow paths passing through the endpoints (P_L and P_R) of the draining line segment (P_LP_R) are chosen to not contribute to the area drained by this line segment. This choice offers the advantage of avoiding surface flow paths shared by draining and nondraining grid cells. In the case shown in Figure 3c (where $r = \arctan(1/4)$), one can obtain that $A_1 = (1/8 + 3/8\ w_1 +$

Table 3. Numerical Features of the Four Simple Cases Shown in Figure 3

Case	r (rad)	α_1 (rad)	α_2 (rad)	w_1	w_2	A_1/h^2	A_2/h^2	A_3/h^2	E_1	E_2
a	0.245	0.000	0.785	1.000	0.000	0.500	1.500	0.500	0.000	0.500
b	0.464	0.785	0.000	0.000	1.000	1.000	1.250	0.250	0.333	0.556
c	0.245	0.245	0.540	0.688	0.312	1.022	0.978	0.398	0.312	0.710
d	0.464	0.464	0.322	0.410	0.590	1.000	1.250	0.250	0.333	0.556

$3/2\ w_2 + 5/8\ w_1\ w_2 + 3/8\ w_2^2)\ h^2$, $A_2 = (7/8\ w_1 + 3/8\ w_1\ w_2 + 5/8\ w_1^2)\ h^2$, $A_3 = (1/8\ w_1 + 5/8\ w_1\ w_2 + 3/8\ w_1^2)\ h^2$, $E_1 = w_2$, and $E_2 = 1/2 + 1/2\ w_2 + 1/4\ w_1\ w_2$. In the case shown in Figure 3d (where $r = \arctan(1/2)$), one can obtain that $A_1 = h^2$, $A_2 = 5/4\ h^2$, $A_3 = 1/4\ h^2$, $E_1 = 1/3$, and $E_2 = 5/9$.

[24] It is noted here that while solving cases shown in Figures 3a and 3c for $r = 0$ yields $A_1 = 0$, $A_2 = 2\ h^2$, $A_3 = 0$, $E_1 = 0$, and $E_2 = 0$, solving cases Figures 3b and 3d for $r = \pi/4$ rad yields $A_1 = h^2$, $A_2 = 3/2\ h^2$, $A_3 = 0$, $E_1 = 2/5$, and $E_2 = 2/5$. This highlights that type 1 and type 2 errors may occur even when flow directions are correctly computed, owing to the limitation (2) introduced in section 1 (second paragraph), when discussing the D8 method, but actually inherent in the use of gridded elevation data. It may therefore be summarized that (1) the same drainage area may be obtained for a given draining line segment by accumulating elementary contributions along different drainage basins and different flow paths (e.g., case shown in Figure 3a with $r > 0$, which yields $E_1 = 0$ but $E_2 > 0$), and (2) correct surface flow paths are obtained if, but not only if (e.g., case shown in Figure 3b with $r = \pi/4$, which yields $E_1 > 0$ and $E_2 > 0$), the condition $E_2 = 0$ (which also implies $E_1 = 0$) is met for all the draining line segments within the drainage basin.

4. Case Studies

[25] The algorithm presented in section 2 is evaluated using the methods developed in section 3 and the elevation data of the Col Rodella area (Eastern Alps, Italy) shown in Figure 4a. The center of the Col Rodella area has latitude 46°29′44″N and longitude 11°45′40″E. In this area, elevation ranges from 1836.7 to 2536.4 m above sea level (asl) with average of 2201.4 m asl. The average terrain slope is 59.3%. Terrain slope is expected to affect the precision with which the terrain morphology is described by contour or gridded elevation data, but it is not expected to directly affect the way in which surface flow paths are determined. On the other hand, the way in which surface flow paths are determined is clearly affected by the terrain plan curvature. In this perspective, drainage systems displaying different morphology in terms of plan curvature are selected in the area shown in Figure 4a to provide a representative set of case studies for the evaluation of algorithms presented in section 2.

4.1. Gridded and Contour Elevation Data

[26] The digital topography of the Col Rodella area was generated from a lidar (light detection and ranging) survey carried out by Terrapoint (United States). Lidar technology is able to provide much more information than can be acquired economically by virtually any other means [*Terrapoint USA Inc.*, 2005; *Carter et al.*, 2007]. The survey was carried out using an airborne lidar terrain mapping (ALTM) system of Terrapoint's proprietary design, mounted on a fixed-wing aircraft. The flight altitude was about 1000 m above ground level (agl) and the acquisition parameters were set to obtain an average data density of about 0.5 points per square meter. The positions of a large number of land surface points (determined with absolute accuracy of 1 m and 0.3 m along the horizontal and the vertical direction, respectively) were processed to provide 1-m resolution gridded elevation data. These gridded elevation data were resampled to 5 m and then used to generate contour elevation data with contour interval of 5 m. Since gridded and contour elevation data were generated using the same topographic information, differences in the determination of surface flow paths from gridded and contour elevation data are ascribed to the limitations inherent in the use of a regular grid. Gridded elevation data were also resampled to 10, 50, 100, and 200 m to investigate the response of single and multiple flow direction algorithms to the variation of grid cell size. It is specified here that the ArcGIS ArcToolbox/Spatial Analyst Tools/Generalization/Aggregate command, with an option selected to provide the mean value, was used to resample 1-m gridded elevation data to the coarser resolutions, whereas the ArcGIS Spatial Analyst/Surface Analysis/Contour command was used to generate 5-m contour elevation data from 5-m gridded elevation data.

4.2. Analysis and Results

[27] Drainage systems having different size and morphological features have been selected within the Col Rodella area as shown in Figure 4a. A small convergent drainage basin (denoted as DB) and a divergent slope (denoted as DS) are first considered to investigate the use of single and multiple flow directions over these two different morphological settings. Then, six subbasins (SB1-SB6) are selected within the DB (only part of SB6 is shown in Figure 4b) to evaluate the ability of algorithms to reproduce drainage areas across a drainage basin. In addition, the DS is subdivided into 12 slices (S1-S12, Figures 4c and 4d), each drained by a single grid cell, to evaluate the ability of algorithms to describe the spatial pattern of the drainage area over divergent terrains. A relatively large drainage basin denoted as Pra Rodella (PR in Figure 4a) is finally considered to investigate the response of single and multiple flow direction algorithms to the variation of grid cell size over the values of 5, 10, 50, 100, and 200 m. Drainage areas, mean elevation and mean slope of the selected drainage systems are reported in Table 4. These drainage systems cover a representative set of cases in order to investigate the role of terrain morphology, drainage basin size, and grid resolution. The ability of flow direction algorithms to determine the drainage divides and surface flow paths along morphologically convergent terrains is especially investigated by considering drainage basins. Drainage basin size and grid resolution are factors that can be varied in this phase. The ability of flow direction algorithms to describe drainage systems having a width

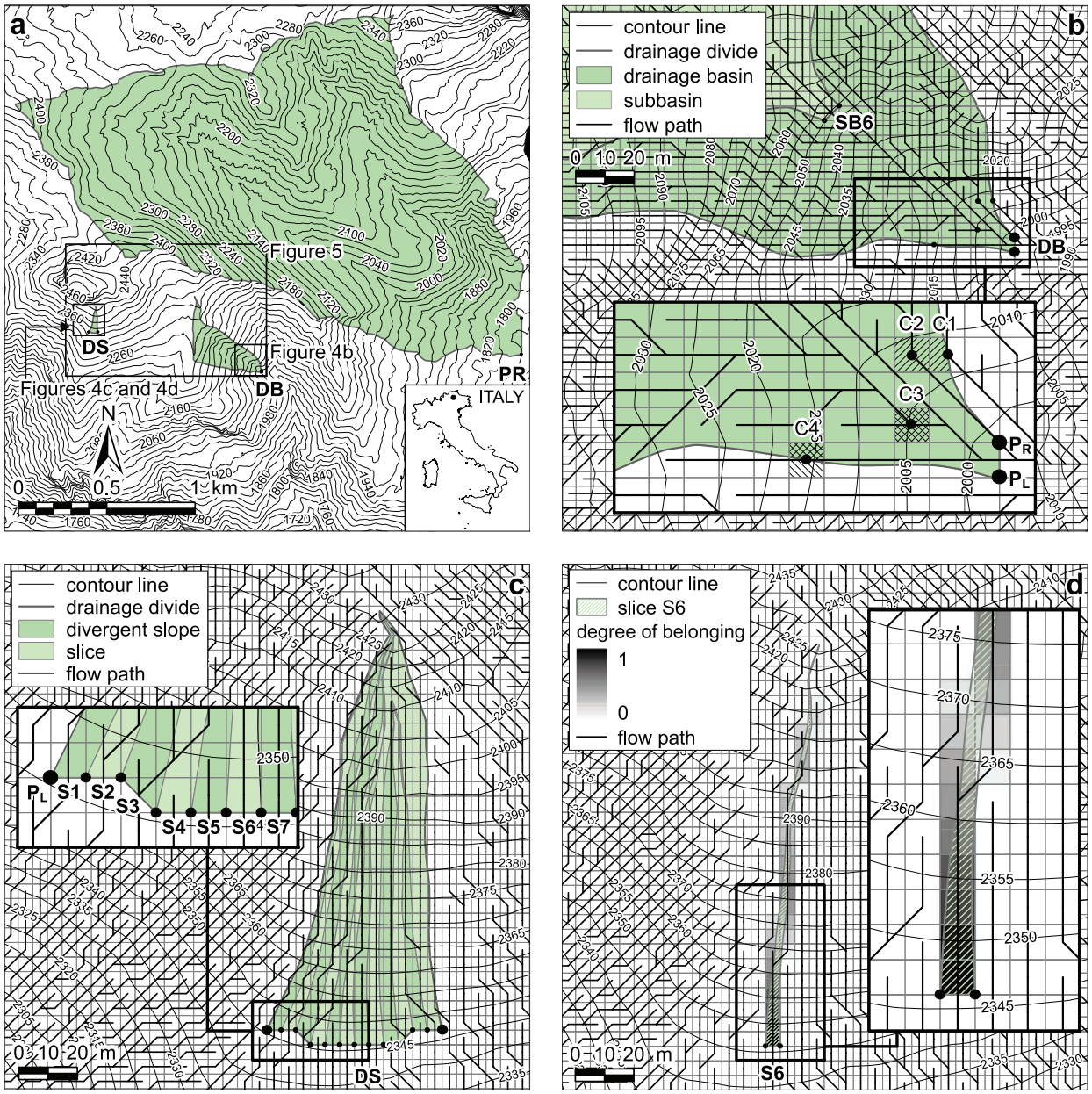

Figure 4. (a) Topographic map of the Col Rodella area (46°29′44″N, 11°45′40″E). (b–d) Comparison between the drainage basins delineated from contour elevation data (using the methods described by *Moretti and Orlandini* [2008]) and the surface flow paths determined from gridded elevation data (using the D8-LTD method described in section 2) for a portion of the drainage basin DB (Figure 4b), the divergent slope DS (Figure 4c), and one of the slices (the slice S6) into which the divergent slope DS is subdivided (Figure 4d). The grid cell size is 5 m. The contour interval is 20 m in Figure 4a and 5 m in Figures 4b–4d. The datum is mean sea level. Numerical features of the drainage systems are reported in Table 4.

comparable to the draining line segment length, and to reproduce the spatial pattern of drainage areas across morphologically divergent terrains is especially investigated by considering slopes. Slope size and grid resolution are factors that cannot readily be varied in this phase owing to the inherent limits in the size of natural slopes.

[28] Drainage divides delineated from contour elevation data (using the methods developed by *Moretti and Orlandini* [2008]) and surface flow paths determined from gridded elevation data (using the algorithms presented in section 2) are shown in Figures 4b–4d for the DB and the DS. Since a clear representation of surface flow paths obtained from a multiple flow direction algorithm is not achieved, surface flow paths shown in Figures 4b–4d are those obtained from a single flow direction algorithm (namely, the D8-LTD method). Examples of elementary contributions to areas A_1, A_2, and A_3 defined in section 3 are highlighted in Figure 4b, where part of the DB and of the SB6 are considered. Cell C1,

Table 4. Physiographic Features, Grid Cell Sizes, and Relative Errors on Drainage Areas for the Drainage Systems Considered in Section 4

Drainage System	Area A[a] (m^2)	Mean Elevation (m asl)	Mean Slope (%)	Grid Cell Size h (m)	$h/A^{0.4}$[b] ($m^{0.2}$)	D8-LTD		D∞-LTD	
						E_1[c] (%)	E_2[c] (%)	E_1[c] (%)	E_2[c] (%)
DB	68,225.8	2,171.5	65.6	5	0.06	2.2	8.5	0.9	**12.1**
SB1	914.1	2,292.8	28.0	5	**0.33**	**20.7**	**40.9**	**60.1**	**92.0**
SB2	5,070.4	2,280.6	33.2	5	**0.16**	6.8	**17.5**	**56.6**	**64.8**
SB3	11,148.6	2,264.3	40.0	5	0.12	2.9	8.3	**10.5**	**19.4**
SB4	19,396.8	2,239.9	54.1	5	0.10	1.8	7.6	5.6	**18.7**
SB5	38,501.5	2,217.7	60.6	5	0.07	2.9	6.6	3.6	**18.5**
SB6	58,376.7	2,194.1	62.2	5	0.06	1.0	3.8	**12.8**	**18.2**
DS	4,659.6	2,378.6	57.2	5	0.17	0.9	**12.3**	6.0	**27.7**
S1	226.5	2,370.5	59.3	5	**0.57**	**54.5**	**135.1**	**105.2**	**229.9**
S2	367.5	2,382.8	54.4	5	**0.47**	**52.4**	**95.9**	**36.5**	**125.8**
S3	445.4	2,376.6	57.4	5	**0.44**	**107.7**	**147.7**	**53.9**	**107.1**
S4	393.7	2,377.7	55.8	5	**0.52**	**91.5**	**93.5**	**63.1**	**102.5**
S5	355.4	2,381.5	55.9	5	**0.48**	**85.9**	**90.4**	5.0	**129.0**
S6	270.2	2,372.7	55.3	5	**0.53**	**94.3**	**127.3**	**43.5**	**147.7**
S7	307.0	2,364.5	57.3	5	**0.51**	**51.1**	**62.7**	7.7	**105.2**
S8	459.9	2,381.7	59.2	5	**0.43**	2.1	**54.8**	**22.3**	**85.8**
S9	438.3	2,376.8	57.1	5	**0.44**	**94.3**	**94.8**	**32.2**	**107.3**
S10	386.7	2,367.2	61.4	5	**0.46**	**68.3**	**156.2**	**75.8**	**99.2**
S11	262.0	2,373.5	59.7	5	**0.54**	**90.5**	**92.3**	**60.9**	**156.1**
S12	847.0	2,389.5	56.4	5	**0.34**	**59.4**	**80.5**	**16.2**	**100.6**
PR	3,186,303.0	2,158.0	44.5	5	0.01	0.8	2.8	0.1	2.5
PR	3,186,303.0	2,158.7	42.4	10	0.03	0.3	1.2	0.5	2.2
PR	3,186,303.0	2,160.8	35.4	50	0.13	0.5	0.9	3.2	8.4
PR	3,186,303.0	2,164.4	30.2	100	**0.25**	2.0	9.0	8.8	**19.2**
PR	3,186,303.0	2,172.6	22.5	200	**0.50**	**29.7**	**43.1**	**52.8**	**61.8**

[a]Area of the drainage system delineated from contour elevation data.
[b]Values of $h/A^{0.4}$ exceeding 0.15 $m^{0.2}$ are highlighted in boldface type.
[c]Values of E_1 and E_2 exceeding 10% are highlighted in boldface type.

draining outside the line segment P_LP_R, partially (i.e., for its proportion belonging to the CDB) contributes to area A_1 (pattern with diagonal lines at $+\pi/4$ rad). Cell C2, draining to the endpoint P_R of the line segment P_LP_R, is conventionally considered to contribute entirely to area A_1 and not to area A_2. Cell C3, draining within the line segment P_LP_R, entirely contributes to area A_2. Cell C4, draining within the line segment P_LP_R, partially (i.e., for its proportion belonging to the CDB) contributes to area A_2 (pattern with crossing diagonal lines at $+\pi/4$ and $-\pi/4$ rad) and partially (i.e., for its complementary proportion not belonging to the CDB) contributes to the area A_3 (pattern with diagonal lines at $-\pi/4$ rad). As shown in Figure 4c, where two shades are used to facilitate the identification of the 12 slices into which the DS is subdivided, the draining line P_LP_R of the DS is drawn in such a way that each slice (S1,S2,. . .) is drained by a single cell with the related surface flow path passing through the center of the cell. The case of a single slice (S6) shown in Figure 4d highlights the need to compute the degree of belonging of each grid cell to the drainage system delineated from contour elevation data in order to ensure a meaningful quantification of areas A_1, A_2, and A_3 introduced in section 3.

[29] The spatial pattern of drainage areas computed using the D8-LTD method, the D∞-LTD method, and a hybrid of the two, obtained by setting the threshold plan curvature K_{ct} equal to zero, are shown in Figures 5a, 5b, and 5c, respectively. The portion of the Col Rodella area selected for this analysis contains both convergent and divergent terrains, as well as complex topographic structures such as ridges, saddles, and peaks (Figure 4a). With respect to single flow direction (nondispersive) algorithms (Figure 5a), pure (Figure 5b) or hybrid (Figure 5c) multiple flow direction (dispersive) algorithms are found to provide a smoother spatial variation of drainage areas. A more in-depth analysis is needed, however, to evaluate algorithms in terms of type 1 and type 2 errors in drainage areas. Path-based methods exhibiting a variable range of dispersive behavior (as obtained by varying the threshold plan curvature K_{ct}) are considered. Local D8 and D∞ methods are also considered in this analysis to assess the improvement offered by the advanced methods presented in this study over the simpler methods currently in use. Results obtained from elevation data with 5 m grid resolution are shown in Figure 6 for the DB and the DS, in Figure 7 for the six subbasins (SB1-SB6) within the DB, and in Figure 8 for the 12 slices (S1-S12) into which the DS is subdivided. Results obtained from elevation data with 5, 10, 50, 100, and 200 m grid resolution describing the drainage basin PR are shown in Figure 9. Type 1 and type 2 relative errors obtained from the D8-LTD and the D∞-LTD methods are also reported in Table 4.

5. Discussion

[30] The results shown in Figure 5 indicate that multiple flow direction (dispersive) algorithms provide a better spatial pattern of the drainage area (Figure 5b) than that provided by single flow direction (nondispersive) algorithms (Figure 5a), which displays numerous source grid cells scattered across the terrain rather than only at ridges, saddles, and peaks. However, the examination of such patterns does not facilitate the evaluation of the underlying

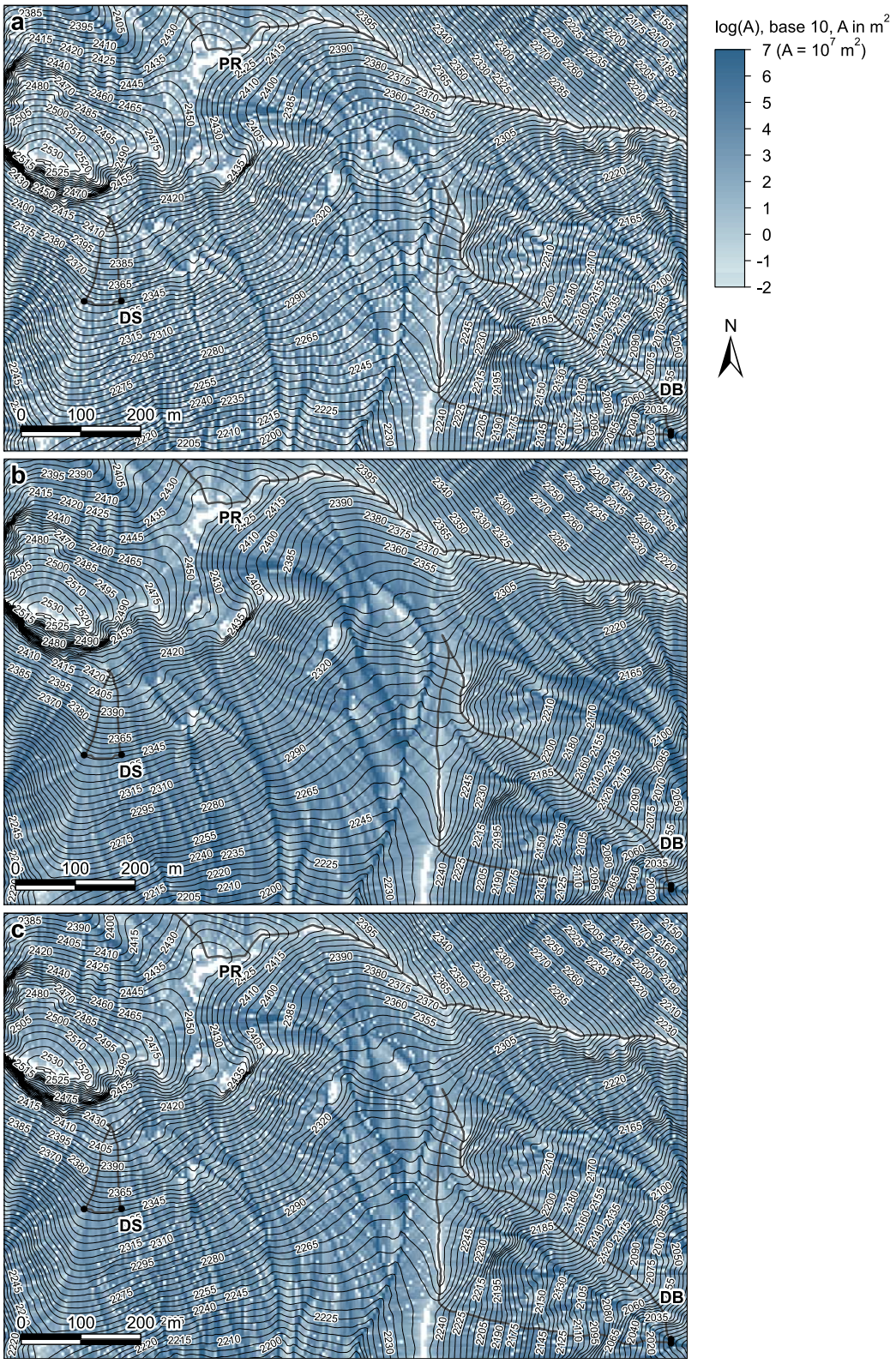

Figure 5. Map of a portion of the Col Rodella area showing logarithmically transformed (base 10) drainage areas contributing to each cell as obtained from (a) the D8-LTD flow direction method, (b) the D∞-LTD flow direction method, and (c) a hybrid of these two methods obtained by setting $K_{ct} = 0$ (section 2). White cells denote source cells with an upslope drainage area equal to zero. The grid cell size is 5 m. The contour interval is 5 m. The datum is mean sea level.

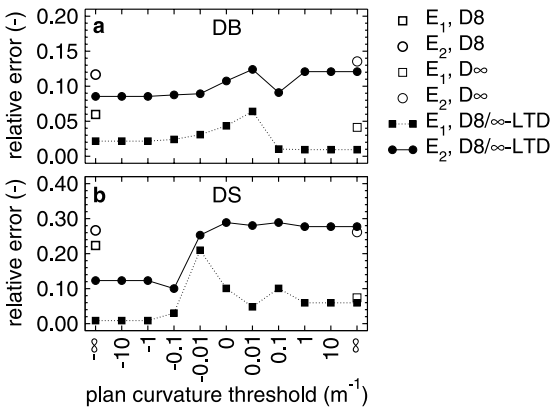

Figure 6. Relative errors in the drainage areas of (a) the drainage basin DB and (b) the divergent slope DS, when gridded elevation data at 5-m resolution are used (Figure 4 and Table 4).

surface flow paths used to actually route flow. The new validation metrics presented in section 3, based on the contributing area overlap and delineation of cells belonging to the contributing flow path, provide a better evaluation of the algorithms intended to provide not only the drainage areas across a terrain, but also a description of surface flow paths.

[31] The results shown in Figure 6 appear to indicate that path-based methods (represented by the hybrid D8/∞-LTD method) generally outperform local methods (represented by the D8 and D∞ methods). The gain in accuracy is especially relevant when nondispersive methods are applied to the DS (Figure 6b). By increasing the amount of dispersion in the determination of flow directions (i.e., by increasing the threshold plan curvature K_{ct}), the accuracy in the determination of drainage areas varies irregularly, revealing the inability to determine a well-defined optimal value for K_{ct}. In the case of the DB, the minimum type 1 error in the drainage area is produced by the D∞-LTD method, but the minimum type 2 error in drainage area is produced by the D8-LTD method (Figure 6a). In the case of the DS, the D8-LTD method is found to provide a satisfactory quantification of the area totally drained by the assigned line in terms of both type 1 and type 2 errors (Figure 6b). Type 1 errors in the total drainage area are reduced by using dispersion when only local methods are considered, but they are not necessarily minimized by using dispersion if path-based methods are also considered. Type 2 errors reported in Figure 6b display a minimum value for $K_{ct} = -0.1$ and slightly greater values if dispersion is not applied ($K_{ct} = -\infty$), revealing that the D8-LTD method essentially provides the most accurate description of surface flow paths over both the drainage basin and the divergent slope. Minimum type 1 errors for the DB and the DS are in the order of few percentage units, whereas minimum type 2 errors are in the order of 10%.

[32] The results shown in Figure 7 indicate that, for a fixed grid cell size (5 m), relative errors in drainage areas generally decrease as the area of the drainage basin increases. The D8-LTD method is found to provide the smallest type 1 and type 2 errors. Using the results shown in Figure 7 and reported in Table 4, one can observe that type 2 (and type 1) relative errors not exceeding 10% are obtained using the D8-LTD method so long as the grid cell size h in meters meets the condition

$$h \leq 0.15A^{0.4}, \tag{13}$$

where A ($A = A_1 + A_2$) is the area of the drainage basin in square meters. Relationship (13) can be explained by assuming that the absolute type 2 error in drainage areas, namely, $E_2 A$, can be estimated as the product of half the grid cell size h by the drainage basin perimeter P, that is $E_2 A \simeq 1/2\, h\, P$. While the well-known relationship $L = 0.32\, A^{0.6}$

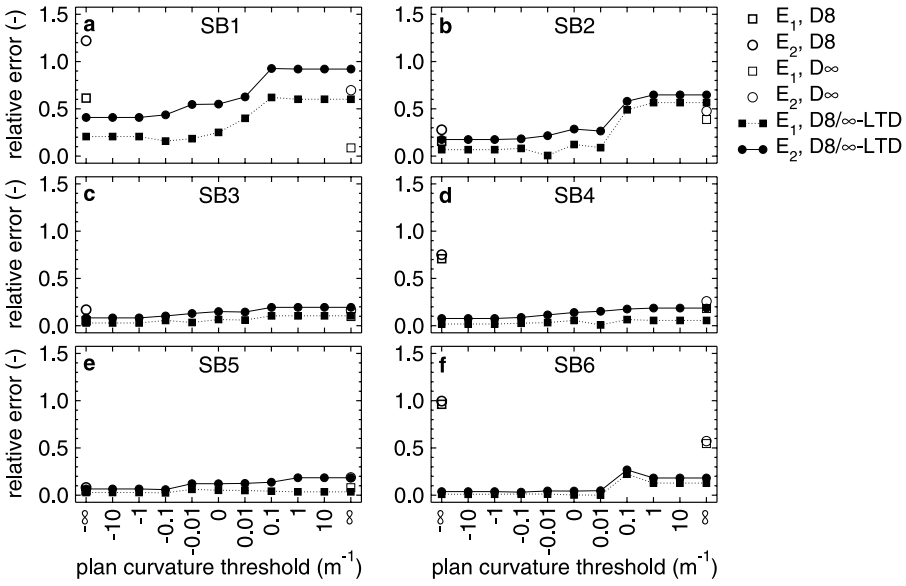

Figure 7. Relative errors in the drainage areas of the six subbasins SB1-SB6 closed by grid cells selected along the main stem of the drainage basin DB, when gridded elevation data at 5-m resolution are used (Figure 4 and Table 4).

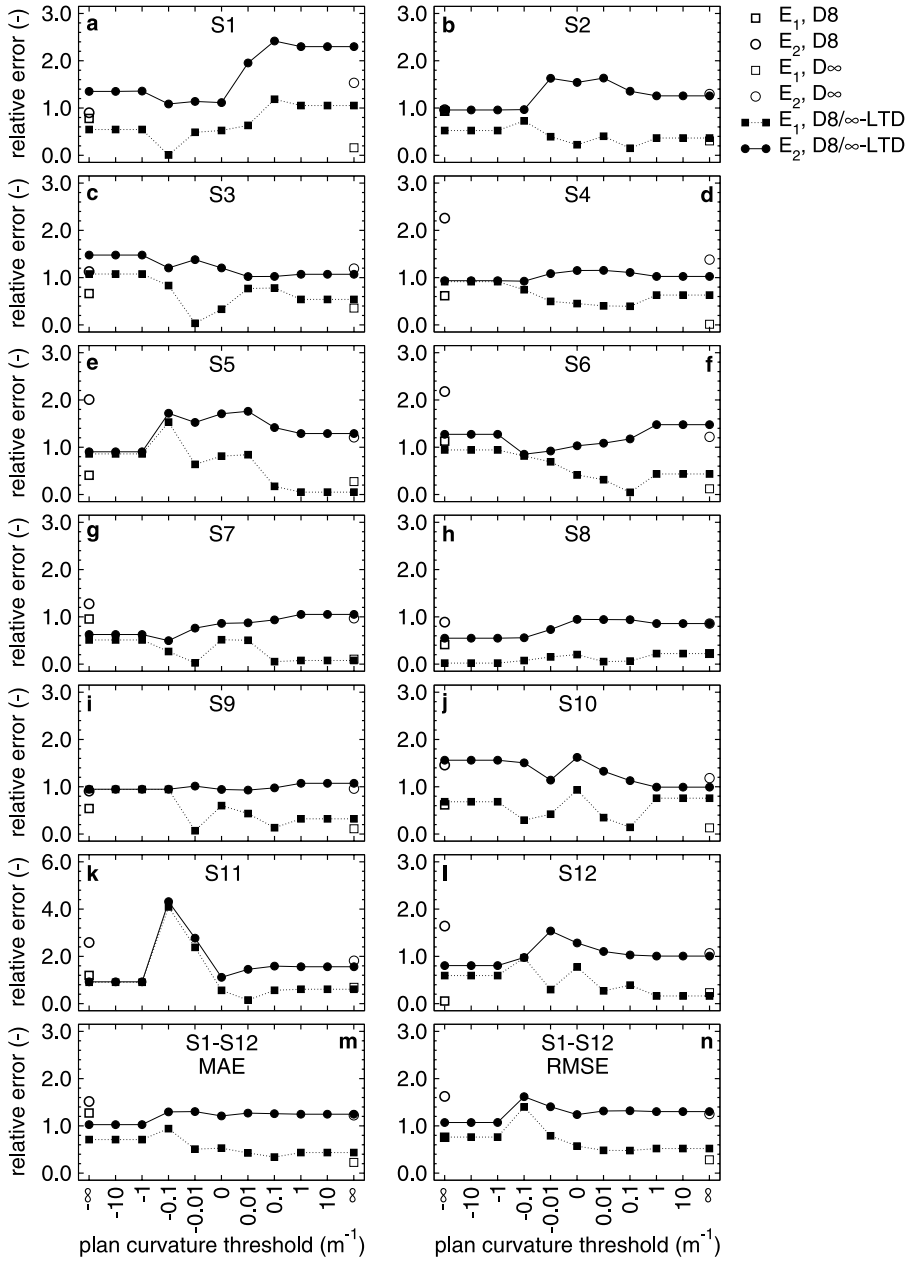

Figure 8. (a–l) Relative errors in the drainage areas of the 12 slices S1–S12 into which the divergent slope DS is subdivided, when gridded elevation data at 5-m resolution are used (Figure 4 and Table 4). (m and n) Mean errors over the 12 slices S1-S12 are expressed in terms of mean absolute error (MAE) and root-mean-square error (RMSE), respectively.

between the mainstream length L in meters and the drainage basin area A in square meters was introduced by *Hack* [1957], a similar relationship between the drainage basin perimeter P in meters and the drainage basin area A in square meters was derived from the analysis of real elevation data by *Cheng et al.* [2001], namely, $P = 1.26\ A^{0.6}$ [*Cheng et al.*, 2001, Figure 8]. Using this relationship, one can obtain that $E_2 \simeq 0.63\ h/A^{0.4}$ and that requirement $E_2 \leq 0.10$ yields relationship (13). Relationship (13) does not always hold for slopes, an occurrence consistent with the fact that Hack's law and the similar law for the drainage basin perimeter are clearly invalid for those systems.

[33] The results shown in Figure 8 reveal that type 1 and type 2 errors in the areas drained by single cells along the DS are approximately 1 order of magnitude larger than those resulting when a draining line segment extending over the mouth of a drainage basin or over more than one cells closing a divergent slope is considered. Improvements offered by path-based methods over the corresponding local methods are observed in terms of mean absolute error (MAE) and root-mean-square error (RMSE) over the 12 slices (Figures 8m and 8n), but exceptions may be observed when slices are considered singularly (e.g., Figure 8a). By varying the amount of dispersion in the determination of flow directions, the accuracy in the determination of drain-

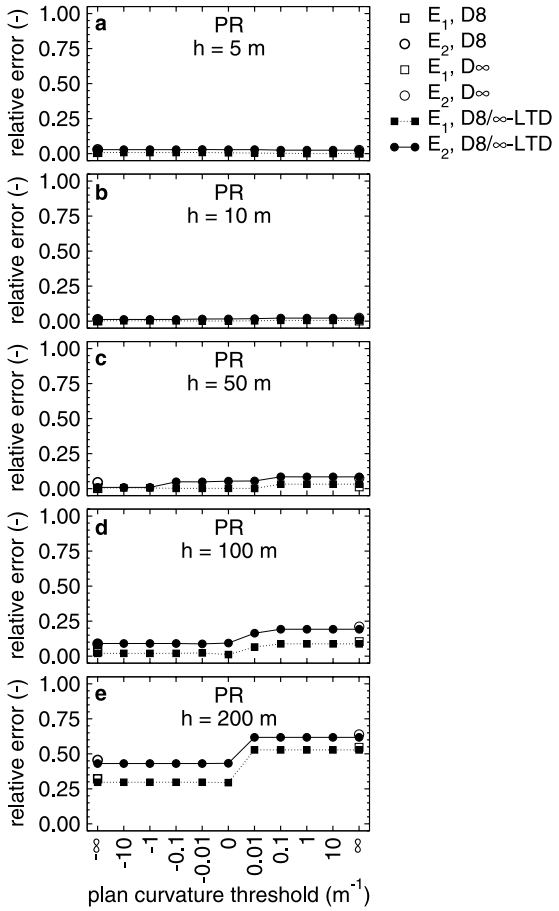

Figure 9. Relative errors in the drainage area of the drainage basin PR, when grid elevation data at resolutions of (a) 5, (b) 10, (c) 50, (d) 100, and (e) 200 m are used (Figure 4 and Table 4).

age areas varies irregularly, revealing also in this case the inability to identify a well-defined optimal value for the plan curvature threshold K_{ct}. Type 1 errors in drainage area are generally found to be reduced by using dispersion, but type 2 errors are generally not significantly affected by it. The analysis over the 12 slices in which the DS is subdivided indicates that dispersion may be useful in describing the spatial pattern of drainage areas across a divergent slope, but reveals that the improvement in the description of drainage areas does not necessarily reflect an improvement in the description of surface flow paths across the divergent slope, which are reproduced equally well (or slightly better) using a path-based, nondispersive method.

[34] The results shown in Figure 9a, when compared to those shown in Figure 6a, indicate that, for a given grid cell size (5 m), both type 1 and type 2 errors decrease significantly as the drainage basin size increases. By comparing results obtained for the drainage basin PR when varying the grid cell size, a concomitant increase in both type 1 and type 2 relative errors in drainage area is noted as K_{ct} increases, indicating erroneous identifications of the drainage divide rather than dispersive exchanges along the drainage divide. The errors produced by nondispersive methods are less than 10% for grid resolutions not exceeding 100 m (Figure 9a–9d and Table 4), whereas errors may reach values as large as 43.1%, for a grid resolution equal to 200 m (Figure 9e and Table 4). A grid size not exceeding 50 m (instead of 100 m) should be used to keep errors below 10%, in case a dispersive or hybrid flow direction method is preferred (Figures 9c and 9d and Table 4). The results obtained for the drainage basin PR reinforce relationship (13).

6. Summary and Conclusions

[35] Multiple flow direction (dispersive) methods (LAD with $\lambda = 0$ or LTD with $\lambda = 1$, $K_{ct} \geq \max(K_c)$ in Table 2) are found to provide a better spatial pattern of the drainage area than that provided by single flow direction (nondispersive) methods (LAD with $\lambda = 0$ or LTD with $\lambda = 1$, $K_{ct} < \min(K_c)$ in Table 2), which displays numerous source grid cells scattered across the terrain rather than only at ridges, saddles, and peaks (Figure 5). The validation metrics presented in section 3, however, reveal that path-based nondispersive methods (LTD with $\lambda = 1$, $K_{ct} < \min(K_c)$ in Table 2) are equally or even more accurate than the dispersive methods in the description of surface flow paths along both convergent drainage basins (Figures 6a, 7, and 9 and Table 4) and divergent slopes (Figures 6b and 8 and Table 4). Numerical experiments carried out on drainage basins by varying the area A (with fixed grid cell size h; Figure 7 and Table 4) and the grid cell size h (with fixed area A; Figure 9 and Table 4) indicate that type 2 errors not exceeding 10% may be expected if $h \leq 0.15\, A^{0.4}$ (h in m and A in m^2). This criterion is not necessarily valid for divergent slopes. Results obtained for divergent slopes drained by line segments having a length comparable to the grid cell size indicate that the best computations of drainage area are provided by dispersive methods with type 1 mean absolute errors exceeding 10% (Figures 8m and 8n and Table 4), and that the best description of surface flow paths are provided by path-based nondispersive methods with type 2 mean absolute errors exceeding 100% (Figure 8m and 8n and Table 4). Type 2 errors in the order of 10% may, however, be expected by using path-based nondispersive methods when a divergent slope drained by more than one grid cell is globally considered (Figure 6b and Table 4).

[36] The analysis carried out in this study suggests that dispersive methods may be preferred over nondispersive methods if the computation of the spatial pattern of the drainage area, especially along divergent terrains, is the main focus. Type 1 mean errors that exceed 10% in areas drained by single grid cells should however be expected in this case. On the other hand, path-based nondispersive methods should be preferred over dispersive methods if the delineation of drainage systems and surface flow paths is an important focus. Type 2 errors not exceeding 10% may be expected in the description of drainage basins and subbasins having area A, provided that high-accuracy gridded elevation data with resolution $h \leq 0.15\, A^{0.4}$ (h in m and A in m^2) are used. In addition, divergent slopes drained by more than one grid cell should be globally considered in order to ensure type 2 errors in the order of 10%. This constraint appears bearable within the general context of terrain analysis, where accurate computations of drainage areas on a regular mesh cannot be obtained even by considering flow nets constructed from contour elevation data due to the limitations mentioned in the first paragraph of section 1. It is concluded that path-based nondispersive

methods are a reliable means for the determination of surface flow paths from gridded elevation data, and provide a sound morphological basis for the distributed description of gravity-driven processes. Further work is needed to formulate models of physical dispersion for water, sediments, and solutes upon this basis.

7. Availability

[37] The FORTRAN 90 code implementing the methods presented in this paper is freely available from the authors under the GNU General Public License agreement.

[38] **Acknowledgments.** The lidar survey of the Col Rodella area (Eastern Alps, Italy) was carried out under the research program PRIN 2001 (grant 2001083841) funded by the Italian Ministry of University and Research. The authors thank Maurizio Cingi (Enìa, Italy) for advice during the development of the FORTRAN 90 code and Claudio Paniconi (INRS-ETE, Université du Québec, Canada) for helpful comments on an early version of the manuscript. The authors are grateful to the three anonymous reviewers for comments that led to improvements in the manuscript.

References

Carter, W. E., R. L. Shrestha, and K. C. Slatton (2007), Geodetic laser scanning, *Phys. Today*, *60*(12), 41–47, doi:10.1063/1.2825070.

Cheng, Q., H. Russell, D. Sharpe, F. Kenny, and P. Qin (2001), GIS-based statistical and fractal/multifractal analysis of surface stream patterns in the Oak Ridges Moraine, *Comput. Geosci.*, *27*(5), 513–526.

Costa-Cabral, M., and S. J. Burges (1994), Digital elevation model networks (DEMON): A model of flow over hillslopes for computation of contributing and dispersal areas, *Water Resour. Res.*, *30*(6), 1681–1692.

Dawes, W. R., and D. Short (1994), The significance of topology for modeling the surface hydrology of fluvial landscapes, *Water Resour. Res.*, *30*(4), 1045–1055.

Fairfield, J., and P. Leymarie (1991), Drainage networks from grid digital elevation models, *Water Resour. Res.*, *27*(5), 709–717.

Freeman, T. G. (1991), Calculating catchment area with divergent flow based on a regular grid, *Computat. Geosci.*, *17*(3), 413–422.

Gallant, J. C., and J. P. Wilson (2000), Primary topographic attributes, in *Terrain Analysis: Principles and Applications*, edited by J. P. Wilson and J. C. Gallant, pp. 51–85, John Wiley, New York.

Hack, J. T. (1957), Studies of longitudinal stream profiles in Virginia and Mryland, *U.S. Geol. Surv. Prof. Pap.*, *294-B*.

Ivanov, V. Y., E. R. Vivoni, R. L. Bras, and D. Entekhabi (2004), Catchment hydrologic response with a fully distributed triangulated irregular network model, *Water Resour. Res.*, *40*, W11102, doi:10.1029/2004WR003218.

Lea, N. L. (1992), An aspect driven kinematic routing algorithm, in *Overland Flow: Hydraulics and Erosion Mechanics*, edited by A. J. Parsons and A. D. Abrahams, pp. 393–407, Chapman and Hall, New York.

Leopold, L. B., M. G. Wolman, and J. P. Miller (1964), *Fluvial Processes in Geomorphology*, W. H. Freeman, San Francisco, Calif.

Marks, D., J. Dozier, and J. Frew (1984), Automated basin delineation from digital elevation data, *GeoProcessing*, *2*(4), 299–311.

Maxwell, J. C. (1870), On hills and dales, *Philos. Mag. J. Sci.*, *4/40*(269), 421–427.

Moore, I. D., and R. B. Grayson (1991), Terrain-based catchment partitioning and runoff prediction using vector elevation data, *Water Resour. Res.*, *27*(6), 1177–1191.

Moretti, G., and S. Orlandini (2008), Automatic delineation of drainage basins from contour elevation data using skeleton construction techniques, *Water Resour. Res.*, *44*, W05403, doi:10.1029/2007WR006309.

O'Callaghan, J., and D. M. Mark (1984), The extraction of drainage networks from digital elevation data, *Comput. Vision Graphics Image Processes*, *28*(3), 323–344.

Orlandini, S., and R. Rosso (1998), Parameterization of stream channel geometry in the distributed modeling of catchment dynamics, *Water Resour. Res.*, *34*(8), 1971–1985.

Orlandini, S., G. Moretti, M. Franchini, B. Aldighieri, and B. Testa (2003), Path-based methods for the determination of nondispersive drainage directions in grid-based digital elevation models, *Water Resour. Res.*, *39*(6), 1144, doi:10.1029/2002WR001639.

Quinn, P., K. Beven, P. Chevallier, and O. Planchon (1991), The prediction of hillslope flow paths for distributed hydrological modeling using digital terrain models, *Hydrol. Processes*, *5*(1), 59–80.

Seibert, J., and B. L. McGlynn (2007), A new triangular multiple flow direction algorithm for computing upslope areas from gridded digital elevation models, *Water Resour. Res.*, *43*, W04501, doi:10.1029/2006WR005128.

Tarboton, D. G. (1997), A new method for the determination of flow directions and upslope areas in grid digital elevation models, *Water Resour. Res.*, *33*(2), 309–319.

Terrapoint USA Inc. (2005), *A White Paper on LiDAR Mapping*, 10 pp., Terrapoint USA Inc., The Woodlands, Tex.

Zevenbergen, L. W., and C. R. Thorne (1987), Quantitative analysis of land surface topography, *Earth Surf. Processes Landforms*, *12*(1), 47–56.

G. Moretti and S. Orlandini, Dipartimento di Ingegneria Meccanica e Civile, Università degli Studi di Modena e Reggio Emilia, Via Vignolese 905, I-41100 Modena, Italy. (giovanni.moretti@unimore.it; stefano.orlandini@unimore.it)